

## ACKNOWLEDGMENTS

We would like to thank R. I. Schermer at Brookhaven for performing some of the required machine calculations, and J. J. Krebs and E. Prince at NRL and

several workers at Bell Telephone Laboratories for useful discussions. Thanks are due to W. U. Tilly and L. G. Paldy for preparing the samples and assisting with the data taking.

Dissociation of  $\text{Li}^{6\dagger}$ 

R. W. OLLERHEAD,\* C. CHASMAN,† AND D. A. BROMLEY

*Yale University, New Haven, Connecticut*

(Received 28 October 1963)

Interactions of  $\text{Li}^6$  ions with carbon and nickel targets have been investigated at incident  $\text{Li}^6$  energies of 36 and 63 MeV, utilizing a  $(dE/dx) \times E$  product identification system capable of separating individual product isotopes. Contrary to expectations based on previous studies in this laboratory on the  $\text{Li}^6(\text{Li}^6, d)\text{B}^{10}$  reaction at 6 MeV which demonstrated a direct reaction mechanism involving the transfer of an alpha particle, no evidence was obtained in the experiments reported herein for deuteron groups corresponding to population of isolated residual states. Each deuteron energy spectrum exhibited a single broad peak, centered at an energy corresponding to the beam velocity, indicating that a direct dissociation mechanism dominates lithium interactions at these higher energies, thus precluding use of  $\text{Li}^6$  ions at high energies as nuclear spectroscopic probes. The total dissociation cross section for 63-MeV  $\text{Li}^6$  ions on carbon, for example, was found to be 24% of the total geometric cross section. In order to establish whether the  $\text{Li}^6$  dissociation proceeds sequentially through well-defined excited states, the elastic and inelastic scattering both of a  $\text{C}^{12}$  beam from a  $\text{Li}^6$  target, and of a  $\text{Li}^6$  beam from a carbon target, were studied. These data demonstrate that processes wherein binary dissociation follows inelastic excitation of unbound  $\text{Li}^6$  states can account for less than 5% of the observed events. It is concluded that the dissociation mechanism is a direct one, reflecting strong alpha-particle plus deuteron-cluster amplitudes in the  $\text{Li}^6$  wave function. Analysis of the dissociation product angular distributions suggests that the dominant interaction involved in these studies is nuclear scattering of the center of mass of the  $\text{Li}^6$  ion from the target. Preliminary studies on the dissociation of  $\text{Li}^7$  and of  $\text{B}^{10}$  and  $\text{B}^{11}$  have also been carried out; in each case, an alpha particle is again a dominant dissociation product.

## I. INTRODUCTION

EXPERIMENTS<sup>1-6</sup> carried out using  $\text{Li}^6$  ion beams at low incident energies have provided convincing evidence that  $\text{Li}^6$  has a well-developed alpha-particle plus deuteron-cluster structure. It has been generally assumed that this would have important consequences concerning the possible utility of lithium ion induced reactions in the investigation of nuclear structure.

Stripping reactions, induced by these ions, in which the alpha particle or the deuteron is transferred to the target nucleus, offer a valuable and perhaps unique probe for the experimental determination of alpha- or deuteron-reduced widths of bound nuclear states, which cannot be obtained directly from resonant scattering measurements.

One of the initial objectives of the experimental studies reported herein was the measurement of the alpha-particle reduced width for the 7.12-MeV,  $1^-$  state in  $\text{O}^{16}$ . This state is bound, lying 42 keV below the binding energy of an alpha particle in  $\text{O}^{16}$ , and can be formed by  $p$ -wave capture of an alpha particle by  $\text{C}^{12}$ . The alpha-particle width of this state is of vital importance in nucleogenesis studies,<sup>7</sup> since it is the single important parameter that remains unknown in the calculation of the helium burning process in stellar interiors. On the basis of earlier studies<sup>2</sup> in this laboratory and elsewhere<sup>1</sup> on the  $\text{Li}^6(\text{Li}^6, d)\text{B}^{10}$  and  $\text{Li}^7(\text{Li}^6, t)\text{B}^{10}$  reactions, which were shown to proceed through direct transfer of an alpha particle, it was hoped that study of the  $\text{C}^{12}(\text{Li}^6, d)\text{O}^{16}$  reaction would provide a direct determination of this and other reduced widths in  $\text{O}^{16}$ . It was further anticipated that use of higher energy  $\text{Li}^6$  ions

† This work has been supported in part by the U. S. Atomic Energy Commission and forms part of a dissertation submitted by one of the authors (R.W.O.) to the graduate school of Yale University, in partial fulfillment of the requirements for the Ph.D. degree.

\* IBM Fellow, 1962-63. Present address: Department of Nuclear Physics, Oxford University, Oxford, England.

† Present address: Physics Department, Brookhaven National Laboratory, Upton, New York.

<sup>1</sup> G. C. Morrison, Phys. Rev. Letters **5**, 565 (1960); see also *Direct Interactions and Nuclear Reaction Mechanisms*, edited by E. Clementel and C. Villi (Gordon and Breach Publishers, New York, 1963).

<sup>2</sup> D. A. Bromley, K. Nagatani, L. C. Northcliffe, R. Ollerhead, and A. R. Quinton, *Proceedings of the Rutherford Jubilee International Conference*, edited by J. B. Birks (Heywood and Company, Ltd., 1962), p. 597.

<sup>3</sup> M. N. Huberman, M. Kamegai, and G. C. Morrison, Phys. Rev. **129**, 791, (1963).

<sup>4</sup> Pham-Dinh-Lien and L. Marquez, Nucl. Phys. **33**, 202 (1962).

<sup>5</sup> R. K. Hobbie and F. F. Forbes, Phys. Rev. **126**, 2137 (1962).

<sup>6</sup> J. M. Blair and R. K. Hobbie, Phys. Rev. **128**, 2282 (1962).

<sup>7</sup> A. G. W. Cameron (private communication).

than had previously been available would minimize distortion effects and thus facilitate extraction of reduced widths from the experimental data.

During the course of the measurements, however, as will be reported in detail herein, it was found that the Li<sup>6</sup> interactions at higher energies are completely dominated by a binary dissociation mechanism precluding the planned spectroscopic studies.

Recent measurements<sup>8-11</sup> on the quasielastic scattering of high-energy protons by the lithium isotopes have suggested striking differences in the structure of Li<sup>6</sup> and Li<sup>7</sup> and further data on the dissociation of these nuclei is required to elucidate the relative validity of cluster or simple shell-model descriptions of these lithium isotopes. The present measurements have been based on the assumption that a cluster structure would be reflected in an augmented yield of the cluster substructures themselves in reactions which induced binary dissociation. Measurements and analyses of inelastic scattering processes directed toward determination of the dissociation mechanism itself have also been carried out.

In the first series of measurements, energy spectra and angular distributions of deuterons from interactions induced by Li<sup>6</sup> ions incident at energies of 63 and 36 MeV were examined. Because of their very different atomic numbers, hence Coulomb fields, both carbon and nickel targets have been used to examine the relative importance of nuclear and Coulomb interactions in the dissociation process.

The second series of measurements was made on the inelastic scattering of C<sup>12</sup> by a Li<sup>6</sup> target and the inverse inelastic scattering of Li<sup>6</sup> by a C<sup>12</sup> target; this series was designed to establish whether the Li<sup>6</sup> dissociation proceeded sequentially through excitation of well-defined states in Li<sup>6</sup>, and if so, to identify the states involved.

The results of these measurements indicate that the dissociation mechanism completely dominates the C<sup>12</sup>-Li<sup>6</sup> interaction at the energies studied, making it impossible to obtain the initially sought information regarding states in O<sup>16</sup>. Large cross sections for the direct dissociation of Li<sup>6</sup> into an alpha particle and a deuteron by a predominantly nuclear interaction were observed, reflecting a high degree of binary clustering in Li<sup>6</sup>. Preliminary measurements have also been carried out on the similar dissociation of Li<sup>7</sup>, B<sup>10</sup>, and B<sup>11</sup> nuclei.

## II. EXPERIMENTAL PROCEDURE

The reaction products were separated for analysis by a  $(dE/dx) \times E$  particle identification system which has

been described previously.<sup>12,13</sup> This technique is based on the approximate relationship between the energy,  $E$ , of a charged particle traversing matter and its incremental energy loss,  $\Delta E$ ,

$$E \times \Delta E \cong KMZ^2,$$

where  $M$  and  $Z$  are the mass and charge of the particle, and  $K$  is an approximate instrumental constant. The product ions from the target pass through a transmission detector, producing a signal proportional to  $\Delta E$ , and are stopped in a second detector which measures their residual energy  $E$ . An analog pulse multiplier was used to form the product of the  $E$  and  $\Delta E$  signals for each event and thus to provide a signal, proportional to  $MZ^2$ , which uniquely identified each particle species. The ranges of multiplier output signals corresponding to desired particle species were selected by single-channel analyzers, which in turn were used to gate multi-channel analyzers recording energy spectra of the selected isotopes simultaneously.

A high resolution ionization chamber,<sup>12</sup> followed by a commercial semiconductor detector, was used for the detection of lithium and carbon ions in the scattering measurements. A gas counter was used for the transmission detector since it is easily made sufficiently thin for short-range particles, and since it is possible to obtain uniform thickness over the effective counter aperture at this required thickness. This latter is particularly essential in heavy-ion studies.

Because of their much lower specific ionizations and longer ranges, it was necessary to use a different detector system for the hydrogen isotopes observed in the dissociation studies, in order to obtain a large enough  $\Delta E$  signal and a detector sufficiently thick to fully absorb the residual energy  $E$ . The transmission detector used in the latter system was an ORTEC Au-Si surface-barrier detector, with a thickness of 95  $\mu$ , entirely depleted at an applied bias of 42 V. The residual energy detector was a 5-mm-thick, lithium-drifted, gold-surface detector fabricated in this laboratory,<sup>14</sup> capable of stopping 29-MeV protons, 42-MeV deuterons, and 48-MeV tritons when operated with an applied bias of 350 V.

Figure 1 is a block diagram of the electronic instrumentation system used in the measurement. The  $E$  and  $\Delta E$  signals were first amplified by low-noise, gain-of-20 voltage-sensitive preamplifiers ( $P$ ). White cathode followers were used to drive roughly 125 feet of signal cable joining the target and control room areas. Prompt outputs from the double delay line amplifiers (DDA) triggered discriminator circuits (D) timed by the crossover point of the double-ended signal pulses. A 6BN6 coincidence circuit (C) with 1  $\mu$ sec resolving time pro-

<sup>8</sup> J. P. Garron, J. C. Jacmart, M. Riou, C. Ruhla, J. Teillac, C. Caverzasio, and K. Strauch, *Phys. Rev. Letters* **7**, 126 (1961).

<sup>9</sup> J. P. Garron, *Nucl. Phys.* **37**, 126 (1962).

<sup>10</sup> G. Tibell, O. Sundberg, and U. Miklavzic, *Phys. Letters* **1**, 172 (1962).

<sup>11</sup> C. Ruhla, M. Riou, J. P. Garron, J. C. Jacmart, and L. Massonnet, *Phys. Letters* **2**, 44 (1962).

<sup>12</sup> C. E. Anderson, D. A. Bromley, and M. Sachs, *Nucl. Instr. Methods* **13**, 238 (1961).

<sup>13</sup> D. A. Bromley, M. Sachs, and C. E. Anderson, *Proceedings of the Harwell Conference on Nuclear Instrumentation*, edited by J. B. Birks (Heywood and Company, Ltd., London, 1962).

<sup>14</sup> C. Chasman and J. Allen, *Nucl. Instr. Methods* (to be published) (1963); and *Bull. Am. Phys. Soc.* **8**, 398 (1963).

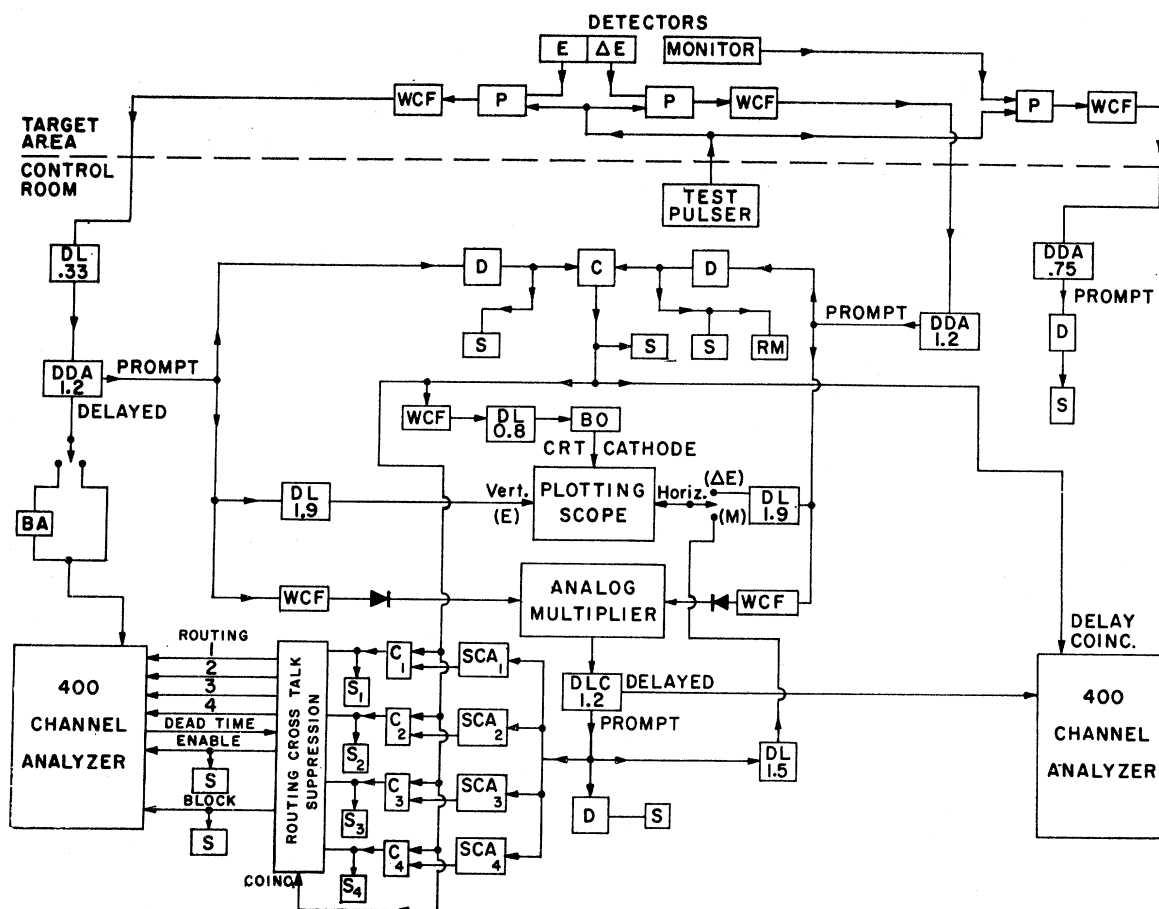


FIG. 1. Block diagram of electronic instrumentation.

vided a pulse used to trigger a blocking oscillator (BO) which applied a negative intensification pulse to the cathode of the CRT in the plotting oscilloscope, in coincidence with the  $E$  and  $\Delta E$  signals applied to the vertical and horizontal deflection plates. A Polaroid camera was used to record each event.

The prompt amplifier outputs were also fed to a diode clipping circuit which coupled the positive portions of the double-ended  $E$  and  $\Delta E$  signal pulses into the analog pulse multiplier. This was a modified version<sup>15</sup> of the instrument described by Stokes<sup>16</sup> and Briscoe<sup>17</sup> based on Raytheon QK-329 squaring tubes. As noted above, the multiplier output pulse provided a signature characteristic of the individual nuclear species. The multiplier output was passed through a delay line clipped amplifier (DCL) to four single-channel analyzers (SCA) used to define regions of the multiplier spectrum for gating purposes. The energy spectra of four different particle species could be recorded simultaneously in

100-channel memory subgroups of the 400-channel analyzer. The pulse-height spectrum of the multiplier output was recorded in another 400-channel analyzer, and the multiplier output was also supplied, in conjunction with the  $E$  signal, to the oscillographic plotting system.

Figure 2 is a typical photograph taken with this system by plotting  $E$  versus  $\Delta E$  for protons and deuterons produced in the bombardment of a polyethylene ( $\text{CH}_2$ ) target by 63-MeV  $\text{Li}^6$  ions. The two groups evident in the proton locus (closest to the origin) correspond to recoil protons from the elastic and inelastic ( $Q = -2.184$  MeV) scattering of the  $\text{Li}^6$  ions from target hydrogen.

The multiplier circuit used here provided two variable parameters which corresponded physically to corrections for dead-layer losses in the detectors, and for the fact that  $\Delta E$  was not a truly differential energy loss. Adjustment of these parameters<sup>15</sup> produced an output pulse with an amplitude proportional to  $MZ^2$  for each isotope.

Figure 3 demonstrates the performance of the system, using semiconductor detectors, in the separation of

<sup>15</sup> M. Sachs, C. Chasman, J. Allen, J. Poth and D. A. Bromley, Nucl. Instr. Methods (to be published).

<sup>16</sup> R. H. Stokes, Rev. Sci. Instr. 31, 768 (1960).

<sup>17</sup> W. L. Briscoe, Rev. Sci. Instr. 29, 5 (1958).

hydrogen isotopes from 36-MeV  $\text{Li}^6$  interactions with a carbon target. The upper figure is an oscillographic photograph, illustrating the straight-line loci obtained, perpendicular to the multiplier axis, while the spectrum displayed below it was obtained from pulse-height analysis of the multiplier output. In addition to providing an identifying signal for any chosen isotopes, the multiplier spectrum also provides a direct measure of the integrated isotopic yields from the reaction under study. In this particular example, an extremely small yield of tritons is evident both in the photograph and in the spectrum.

Figure 4 is a calibration proton spectrum obtained by bombarding a polyethylene ( $\text{CH}_2$ ) target with 63-MeV  $\text{Li}^6$  ions. The sharply defined groups correspond to recoil protons from elastic and inelastic scattering of lithium by the hydrogen in the target, are also evident in the corresponding photograph shown as Fig. 2. The demonstrated energy resolution of approximately 1% was due chiefly to spread in the beam energy, with small contributions from straggling in the target and transmission counter. The 5-mm  $E$  detector itself had a measured

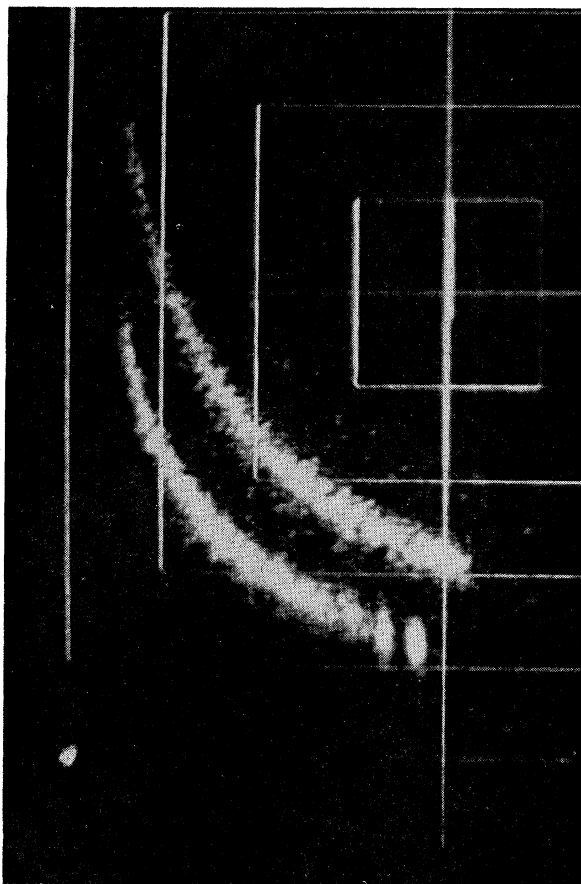


FIG. 2. Plotting oscilloscope photograph of  $\Delta E$  versus  $E$  for the 63-MeV  $\text{Li}^6$  bombardment of a polythene ( $\text{CH}_2$ ) target. Much longer exposure times would have been required to show a similar triton locus. (See Fig. 3.)

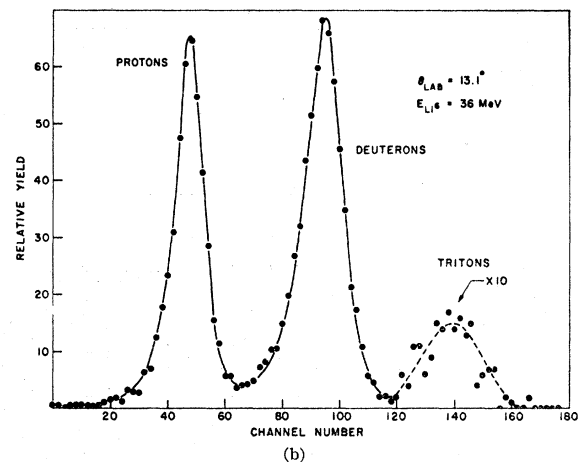
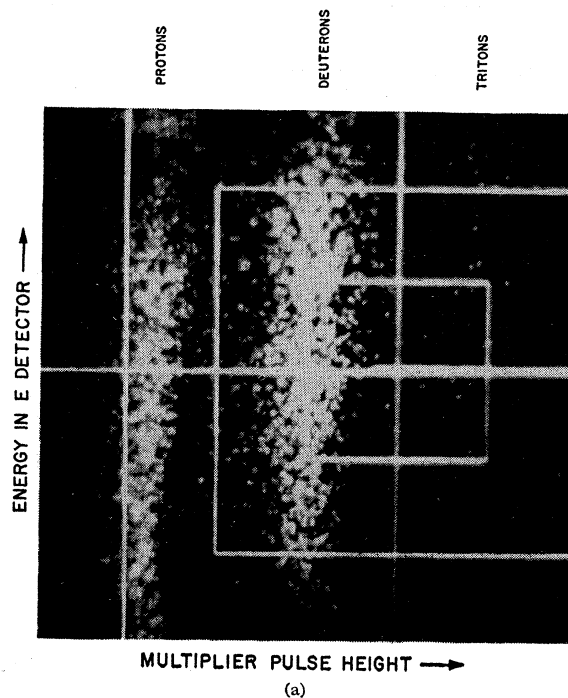


FIG. 3. (a) Oscillographic and (b) spectra displays of the multiplier response to the hydrogen isotopes produced in the 36-MeV  $\text{Li}^6$  bombardment of  $\text{C}^{12}$ .

resolution of 80 keV, including all instrumental effects, when tested at room temperature with the 5.5-MeV alpha particles from an  $\text{Am}^{241}$  source.

In the scattering experiments, energy calibrations were obtained by observing the elastic scattering of the beam by a thin gold target.

The  $\text{Li}^6$  target was prepared by vacuum evaporation onto a 0.000025-in. nickel foil, so that in the scattering of  $\text{C}^{12}$  from  $\text{Li}^6$ , an additional energy calibration for each spectrum was provided by the elastic scattering peak from the nickel backing. A biased amplifier was used for the scattering measurements in order to expand the energy spectra by as much as a factor of 5 to

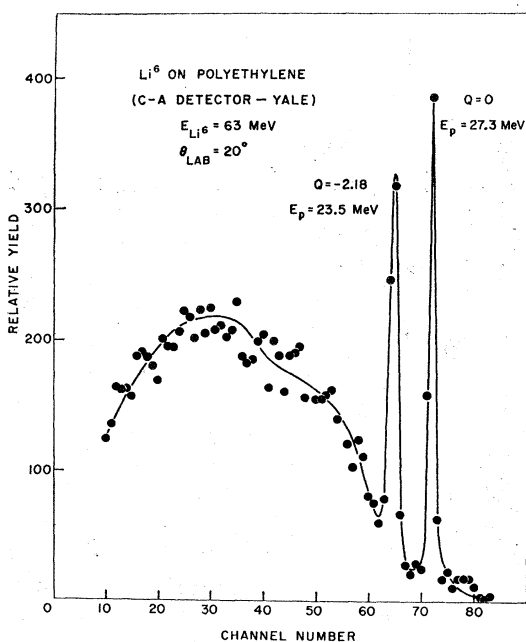


FIG. 4. Proton energy spectrum used for system energy calibration.

obtain improved energy resolution. The carbon target was self-supporting and was also prepared by vacuum evaporation. Areal densities of  $0.21 \pm 0.02$  and  $1.4 \pm 0.3$  mg/cm<sup>2</sup> were measured for the carbon and Li<sup>6</sup> targets, respectively.

### III. EXPERIMENTAL RESULTS

#### A. Energy Spectra

Typical energy spectra of the deuterons produced in the Li<sup>6</sup> bombardment of carbon and nickel targets are presented in Figs. 5 and 6. The upper spectrum in each figure was obtained at an incident energy of 36 MeV. As indicated in Fig. 5, the ground-state C<sup>12</sup>(Li<sup>6</sup>,d)O<sup>16</sup> reaction deuteron group for an incident energy of 36 MeV would be expected at an energy of 39.6 MeV; the corresponding group for 63-MeV incident Li<sup>6</sup> ions would appear at 64.6 MeV. Deuterons were not detected at these energies nor as sharp groups corresponding to any of the excited states of O<sup>16</sup>, at either energy, at any angle of observation. It should perhaps be emphasized that this cannot reflect an instrumental defect since, for example, deuterons were detected in the high-incident-energy spectrum at the energies of interest for the low-incident-energy reaction. It was concluded from such measurements that a dissociation mechanism dominates the Li<sup>6</sup>+C<sup>12</sup> interaction at these energies.

The spectra shown here are characteristic of all those measured, at various laboratory angles, in exhibiting a single broad maximum centered at an energy corresponding to the incident beam velocity, reduced slightly by the dissociation energy. The shaded areas in each case indicate the region of energies available to

the deuteron, assuming excitation of the Li<sup>6</sup> to its 2.184-MeV state, and subsequent decay into an alpha particle and deuteron, a mechanism initially considered most reasonable in the dissociation. The shift in the position of the maximum yield in the spectrum corresponding to a change in the incident projectile energy is evident in both figures. It should also be noted that a higher proportion of deuterons lies outside the shaded areas in the spectra taken at higher incident energy. This may be interpreted as merely reflecting the increased amount of energy available to the dissociation products, regardless of the details of the reaction mechanism. For example, if the reaction were to proceed, as noted above, via sequential inelastic excitation and decay, the probability of dissociation via states in Li<sup>6</sup> above the 2.184-MeV level would increase with the incident energy.

#### B. Angular Distributions

Laboratory angular distributions were obtained by summing the deuteron yield at each laboratory angle. These are presented in Figs. 7 and 8 for the carbon and nickel targets, respectively. The vertical bars labeled  $\theta_c$  in each case indicate the angle corresponding to an impact parameter equal to the interaction radius, assum-

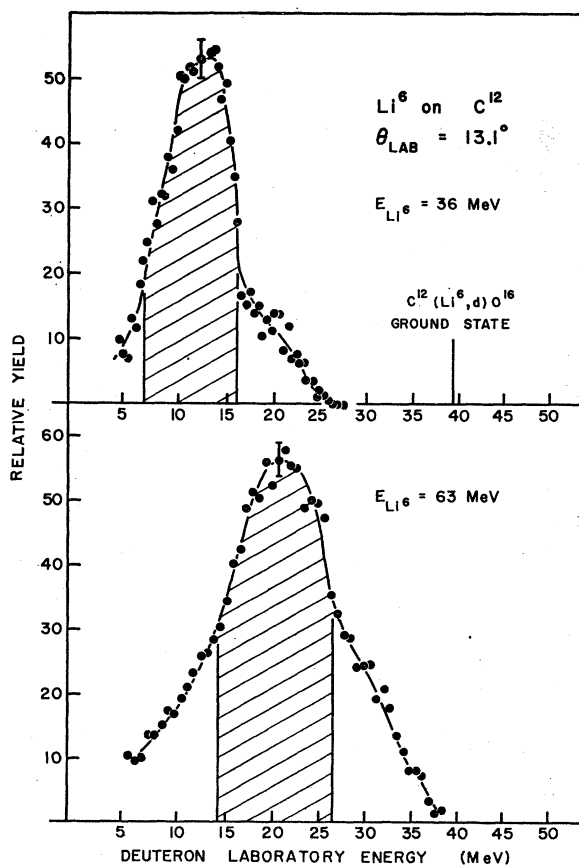


FIG. 5. Deuteron energy spectra from the Li<sup>6</sup> bombardment of a carbon target.

ing classical Rutherford trajectories. As shown in Fig. 7 these angles are too small to be readily accessible experimentally in the case of a  $\text{C}^{12}$  target. It was obviously of considerable interest to establish whether or not the angular distributions had a maximum near this grazing angle, analogous to that characteristically observed in nucleon transfer studies. This also prompted the measurements with a nickel target, in which case, as illustrated, the grazing angle was readily included in the range of observation. As shown in Fig. 8, no evidence for such a maximum was obtained, suggesting that the dissociation does not occur predominantly via a simple grazing collision.

The data of Figs. 7 and 8 show very different energy dependence for the two targets; the cross section is almost independent of energy for the carbon target, whereas it is roughly proportional to energy for the nickel target. The possible significance of this will be discussed below.

**C. Total Cross Sections**

Total cross sections were obtained from the above angular distributions in two ways. As illustrated in

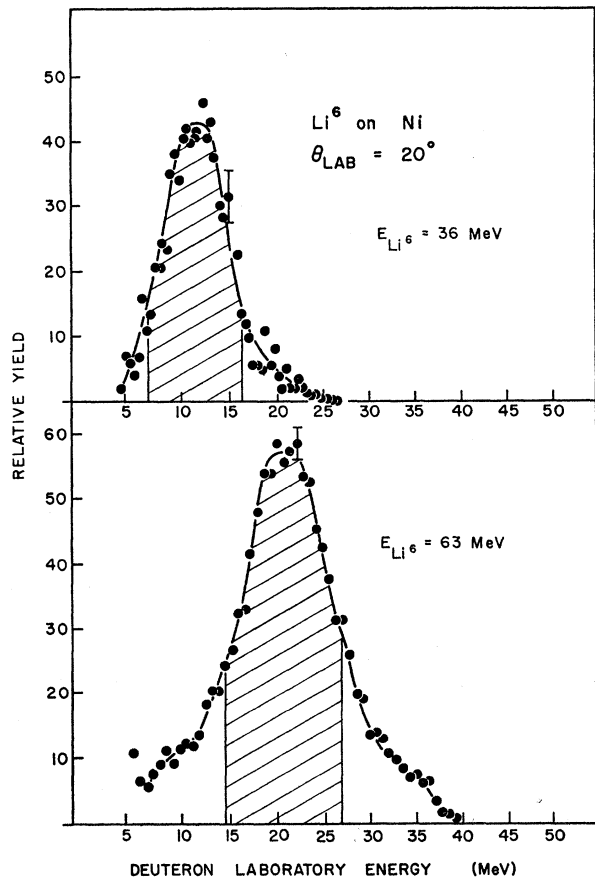


FIG. 6. Deuteron energy spectra from the  $\text{Li}^6$  bombardment of a nickel target.

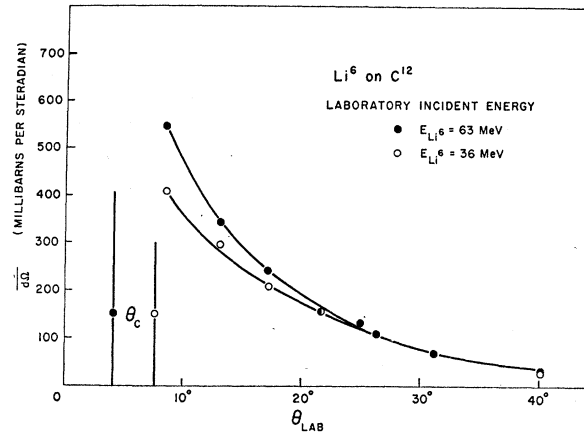


FIG. 7. Deuteron angular distributions from the  $\text{Li}^6 + \text{C}^{12}$  system. The vertical bars labelled  $\theta_c$  in each case indicate the angle corresponding to an impact parameter equal to the interaction radius.

Fig. 9, the angular distributions were very nearly exponential in the range considered. A functional form  $\sigma(\theta) = A e^{-\alpha\theta}$  was therefore fitted to the data; the total cross sections were obtained, by integration, as

$$\sigma_T = \int_0^\pi \sigma(\theta) d\Omega = 2\pi A \frac{1 + e^{-\alpha\pi}}{1 + \alpha^2} \quad (1)$$

The cross section values obtained in this manner, together with the values of the parameters  $A$  and  $\alpha$  determined for each case, are presented in Table I.

The  $\sigma_T$  values were checked by mechanical integration of the curve obtained by multiplying the experimental  $d\sigma/d\Omega$  by the appropriate value of  $\sin \theta$ . Since this method necessitated assuming a shape for the angular distributions in the small angle region, the first method was better standardized, and values thus obtained have been compared with the geometric cross section in Table I. A number of other relevant parameters are also tabulated including the Coulomb barrier

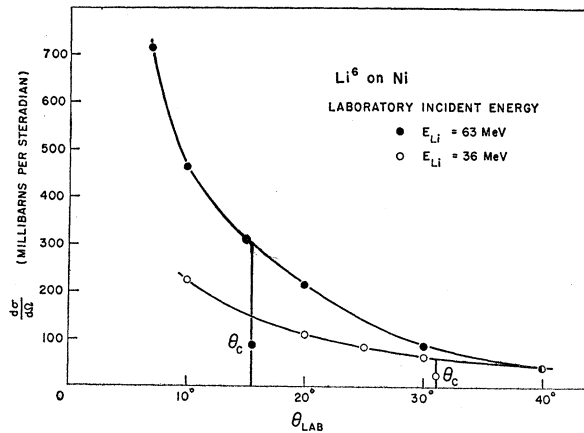


FIG. 8. Deuteron angular distributions from the  $\text{Li}^6 + \text{Ni}$  system. The angle  $\theta_c$  is as defined in the caption of Fig. 7.

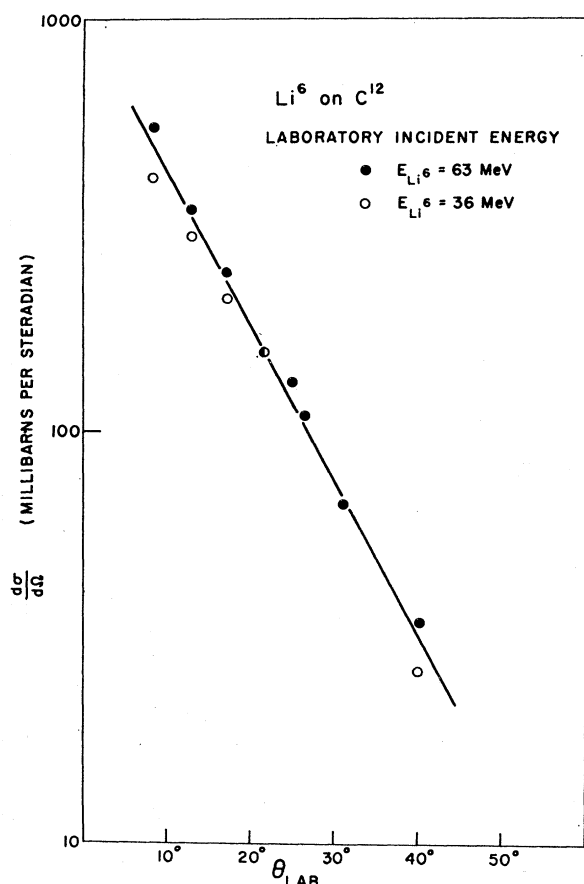


FIG. 9. Deuteron angular distributions illustrating their exponential character and independence on energy.

and the Sommerfeld parameter  $\eta$ , defined by

$$\eta = Z_1 Z_2 e^2 / \hbar v. \quad (2)$$

It should be noted in Table I, that dissociation comprises a surprisingly large fraction of the geometric cross section, except in the case of the lower incident energy  $\text{Li}^6$  ions on Ni where the high value of  $\eta$  is reflected in Coulomb inhibition of the dissociation process responsible for the high cross section in the other cases.

The cross sections, assuming Coulomb excitation of the  $\text{Li}^6$  ions and subsequent decay have also been calcu-

TABLE I. Cross sections and parameters related to the dissociation of  $\text{Li}^6$ .

Target	Carbon	Nickel
$R$ (F)	5.91	8.19
Coulomb barrier (MeV)	4.38	14.8
Incident energy (MeV)	63	63
Center-of-Mass energy (MeV)	42	57
$\eta$	0.88	4.1
Functional parameters	$A$ (mb)	$\alpha$
	1040	915
	4.89	5.05
Integrated cross section $\sigma_T$ (mb)	264	217
Geometric cross section $\sigma_g$ (b)	274	242
	1.10	2.10
$\sigma_T/\sigma_g$	0.24	0.20
Coulomb cross section $\sigma_{E2}$ (mb)	125	76
$\sigma_T/\sigma_{E2}$	2.1	2.9
	0.14	0.085
	334	164
	0.87	1.1

lated in order to compare the present data with previous results<sup>18</sup> for the dissociation of 63-MeV  $\text{Li}^6$  ions by gold. Gluckstern and Breit<sup>19</sup> were successful in obtaining a semiquantitative fit to those data assuming  $E2$  Coulomb excitation of the  $\text{Li}^6$  nucleus to its three lowest  $T=0$  states, predominantly to the 2.184-MeV  $3^+$  level, with subsequent decay of these states into an alpha particle and a deuteron. The Coulomb cross sections are tabulated as  $\sigma_{E2}$  and have been compared to the observed cross sections in the last row of Table I. These comparisons will be discussed below in greater detail.

#### D. Scattering Data

In an attempt to establish whether or not the lithium dissociation does proceed through well-defined excited states of  $\text{Li}^6$ , the scattering of a carbon beam from a  $\text{Li}^6$  target was measured. Since the heavy ion accelerator has a fixed output-beam velocity, the  $\text{Li}^6 + \text{C}^{12}$  center-of-mass system is the same for a fully accelerated beam regardless of which particle is incident. It was recognized that states inelastically excited in  $\text{Li}^6$ , regardless of their decay mode, would be identified by the presence of corresponding well-defined peaks in the energy spectrum of the inelastically scattered carbon with reaction  $Q$  values corresponding to excitations in  $\text{Li}^6$ . The lowest

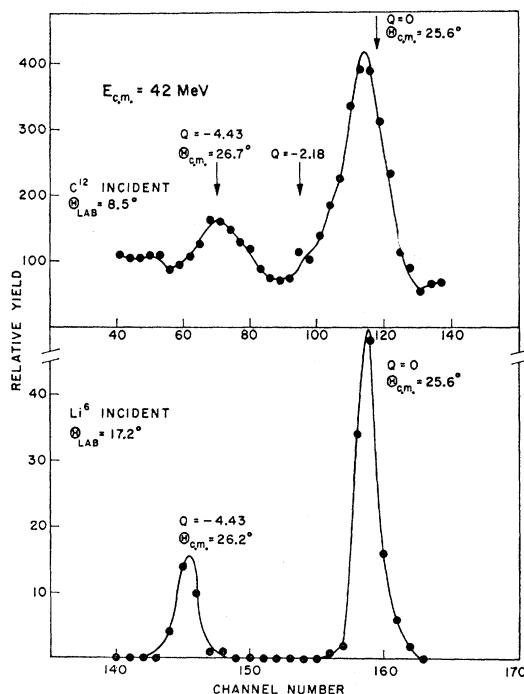


FIG. 10. Energy spectra from  $\text{Li}^6\text{-C}^{12}$  scattering. The upper spectrum corresponds to the observation of  $\text{C}^{12}$  ions scattered by a  $\text{Li}^6$  target and the lower spectrum to observation of  $\text{Li}^6$  ions scattered by a  $\text{C}^{12}$  target at corresponding center-of-mass angles.

<sup>18</sup> C. E. Anderson, in *Reactions Between Complex Nuclei*, edited by A. Zucker, F. Howard, and E. C. Halbert (John Wiley & Sons, Inc., New York, 1961), p. 67.

<sup>19</sup> R. L. Gluckstern and G. Breit, in *Reactions Between Complex Nuclei*, edited by A. Zucker, F. Howard, and E. C. Halbert (John Wiley & Sons, Inc., New York, 1961), p. 77.

excitation in  $\text{C}^{12}$  has a  $Q$  value of  $-4.43$  MeV, so that excitation of the 2.18-MeV state in  $\text{Li}^6$  could be clearly identified, if present.

Typical energy spectra obtained in this manner are presented in the upper half of Figs. 10 and 11. The elastic scattering peak from the nickel backing provided a reliable energy calibration for each spectrum. This peak, not shown in the figures, appeared in the spectra beyond the highest energy shown. The arrows, however, indicate the positions of peaks in the  $\text{Li}^6 + \text{C}^{12}$  scattering spectrum *predicted* from the position of this calibration peak. The elastic ( $Q=0$ ) peak and the inelastic peak corresponding to the first-excited state in carbon ( $Q=-4.43$  MeV) were identified in each spectrum, and angular distributions for these two processes were obtained. No evidence was found for significant inelastic excitation of the 2.184-MeV level in  $\text{Li}^6$ .

These measurements were also repeated by reversing the reaction and using  $\text{Li}^6$  beam on a carbon target, to examine and minimize possible errors in the inelastic scattering measurements with the  $\text{Li}^6$  target. Since  $\text{Li}^6$  is very active chemically, it was very difficult to determine accurately the thickness of the lithium itself, exclusive of any compounds, with a resultant uncertainty in cross section values. The nickel backing and the thickness of the lithium target resulted in poorer energy resolution in the first measurements, as indicated in the figures. Inelastic scattering from the nickel target, though found to be quite small, could have contributed significantly to low cross section regions in the  $\text{C}^{12} + \text{Li}^6$  spectrum.

Energy spectra obtained from the reversed reaction measurements are presented in the lower portions of Fig. 10 and 11. They have been obtained at approximately the same center-of-mass angles as the upper spectra in these figures. The spectra demonstrate that the energy resolution was quite acceptable and that the identifications of the peak origins were certain; the lack of background gave credence to the values obtained for the differential cross sections. It should be noted that in these later measurements a spectral peak corresponding to inelastic excitation of the 2.184 state in  $\text{Li}^6$  would not be expected since this state is not bound against dissociation into a deuteron and alpha particle and in consequence its lifetime is much shorter than the transit time of the excited  $\text{Li}^6$  ion, if present at all, from the target to the detector.

Agreement between measurements in the direct and reversed reactions further served to verify the identification of the peaks in the former case, and substantiated the absolute values obtained for the differential cross sections. Moreover, use of the same carbon target, as utilized for measurement of deuteron production, permitted a very necessary direct comparison of cross sections obtained in the dissociation and inelastic scattering interactions.

Angular distributions obtained from scattering measurements are presented in Fig. 12. The open symbols represent data obtained using the carbon target, with error bars representing statistical uncertainty. The solid lines have simply been drawn through the data points, and do not represent theoretical curves. It will be noted

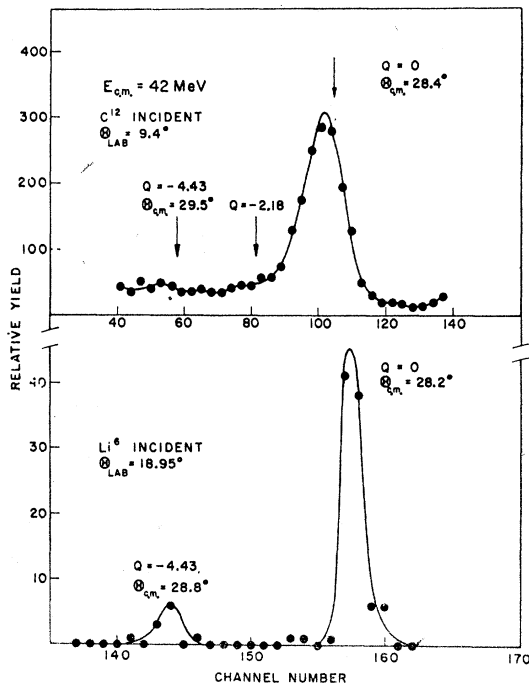


FIG. 11. Energy spectra observed in  $\text{Li}^6\text{-C}^{12}$  scattering. (See caption to Fig. 10.)

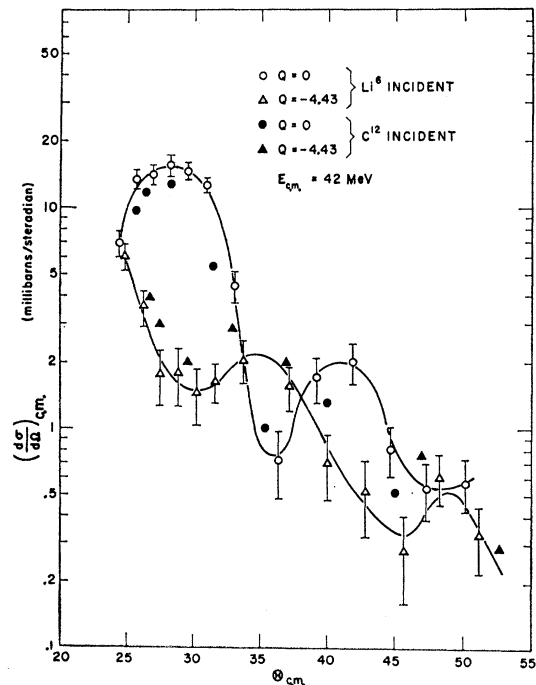


FIG. 12. Angular distributions observed in  $\text{Li}^6\text{-C}^{12}$  scattering.

that the inelastic diffraction pattern is out of phase for inelastic excitation of a state having the same parity as the ground state as required by the well-known Blair rule.

The open and solid symbols represent data points obtained with the  $C^{12}$  and  $Li^6$  targets, respectively. The agreement obtained is gratifying considering the possible uncertainty in the thickness of the lithium target and the probable errors due to spectrum contributions from the nickel backing. The elastic scattering points with the  $Li^6$  target are consistently low, indicating an overestimate of the lithium target thickness, probably reflecting the presence of lithium compounds at the time of weighing. The inelastic scattering cross sections are somewhat high, reflecting the inclusion of contributions from the nickel background.

The agreement is, however, certainly adequate to establish an estimate of an *upper limit* for the differential cross sections for inelastic scattering to the first-excited state in  $Li^6$ . This was obtained by summing the yield in an energy region roughly the width of the elastic peak, between the  $Q=0$  and  $Q=-4.43$  peaks in the energy spectra obtained using the  $Li^6$  target. The corresponding angular distribution is presented in Fig. 13, together with the elastic scattering data from the same spectra for comparison. The deuteron yield from the same incident system is also displayed, transformed to the entrance channel center-of-mass system on the hypothesis (incorrect, but adequate) that all deuterons had an energy corresponding to an inelastically scat-

tered  $Li^6$  with a reaction  $Q$  value of  $-2.184$  MeV. It is clear that disintegration following sequentially on inelastic excitation of the 2.184-MeV state in  $Li^6$  is insufficient, by as much as two orders of magnitude, to account for the observed deuteron yield from the dissociation process.

#### IV. DISCUSSION

##### A. Energy Spectra

As noted above, the deuteron energy spectra exhibited a single broad maximum centered at an energy corresponding roughly to the beam velocity, suggesting a direct dissociation of the incident  $Li^6$  ions.

From simple kinematic arguments it may be shown that particles resulting from the binary dissociation, in flight, of a nucleus in a well-defined excited state, have limits imposed on the energy with which they can appear in the laboratory; with certain simplifying assumptions the shape of the energy spectrum between these limits is also predictable. If a mass  $M$  with laboratory energy  $E_0$  dissociates into two particles of masses  $m$  and  $m'$  with an energy release  $Q$ , and if  $m$  is emitted at an angle  $\varphi$  in the rest frame of  $M$ , with respect to the original direction of motion of  $M$ , then the laboratory energy for  $m$  is given simply by

$$E = E_c + e + 2(eE_c)^{1/2} \cos \varphi, \quad (3)$$

where

$$E_c = \frac{m}{M} E_0 \quad \text{and} \quad e = \frac{m'}{m+m'} Q. \quad (4)$$

The upper and lower limits of  $E$  then correspond to  $\varphi=0$  or  $\pi$ , respectively, and are indicated by the limits of the shaded area in Figs. 5 and 6. The energy widths of the shaded area are given by

$$W = E_{\max} - E_{\min} \sim 4/M (mm' E_0 Q)^{1/2}, \quad (5)$$

and is seen to be quite sensitive to the value of  $Q$ , and therefore to the excitation energy in  $Li^6$  ( $Q=0.71$  MeV for excitation to the 2.18-MeV level in  $Li^6$ ).

If it is assumed that the emission of  $M$  is isotropic in the projectile-target center-of-mass system, and further that the emission of  $m$  is isotropic in the rest frame of  $M$ , the laboratory energy spectrum of  $m$  is predicted to be a rectangular distribution extending between the limits implied by Eq. (1). Anisotropies reflecting, for example, diffraction effects in the scattering of  $M$  and angular momentum effects in the subsequent decay, act to distort the simple rectangular shape. However, the above considerations are useful in estimating the form of the expected distributions, and as illustrated in Figs. 5 and 6, a large part of the deuteron yield does indeed lie within the calculated region.

The laboratory emission angle of the product particle  $m$  can deviate from the original direction of  $M$  by an angle  $\gamma$  obtained from consideration of the velocity

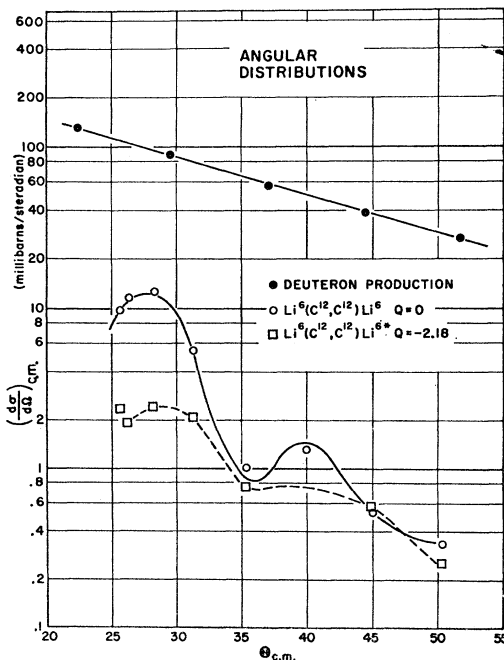


FIG. 13. Angular distributions comparing the deuteron yield from the  $Li^6$  bombardment of  $C^{12}$  to the differential cross sections for inelastic excitation of  $Li^6$  in scattering from  $C^{12}$ .

vectors involved, and given by

$$\gamma = \sin^{-1} \left( \frac{e}{E_c} \right)^{1/2} \quad (6)$$

For 63-MeV Li<sup>6</sup> ions incident on C<sup>12</sup>,  $\gamma = 8.9^\circ$  for emission of  $M$  at a laboratory angle of  $13.1^\circ$ . The corresponding angular deviation in the incident center-of-mass system is  $13.4^\circ$ , independent of the center-of-mass emission angle. Since this is the *maximum* deviation which the deuterons can have from the inelastically scattered Li<sup>6</sup> direction, the maximum effect this could have on the deuteron angular distribution would be to shift it  $13.4^\circ$  from the inelastic scattering direction. It is clear from inspection of Fig. 13 that the large disparity in the magnitudes of the differential cross sections for scattering and deuteron production cannot be accounted for in this manner, assuming sequential excitation and dissociation.

In considering more complex dissociation processes, it was realized that the results might be very dependent on the phase-space volume available to the interacting particles. In consequence, to examine the relevance of such a process, the observed deuteron energy spectra have been compared to the purely statistical energy distribution predicted for the three-body system consisting of alpha particle, deuteron, and target nucleus. This is given by

$$P(E)dE = A[E(E_{\max} - E)]^{1/2}dE, \quad (7)$$

where  $A$  is a constant, and

$$E_{\max} = \frac{m_2 + m_3}{m_1 + m_2 + m_3} T, \quad (8)$$

is the maximum energy which  $m_1$  can have if  $T$  is the total energy available in the center-of-mass system.

The energy spectra of Figs. 5 and 6 obtained at 63-MeV incident energy have been transformed to the entrance channel center-of-mass system utilizing the invariance of the quantity  $E^{-1/2}d^2\sigma/d\Omega dE$ , and are presented as the solid curves in Fig. 14. The corresponding statistical distributions, with the constant,  $A$ , normalized to unity, are indicated by the dashed curves; the experimental and statistical distributions have been normalized to have the same maximum value.

It is evident that the observed spectra do not resemble the continuous distribution predicted by statistical considerations, and are peaked at a much lower energy. Beckner *et al.*<sup>20</sup> have also demonstrated that the inclusion of Coulomb effects suppresses the low energy end of the statistical spectrum, an effect which would further enhance this disagreement. These considerations indicate that statistical phenomena cannot be important in the interactions studied.

The various possible two-body interactions for the

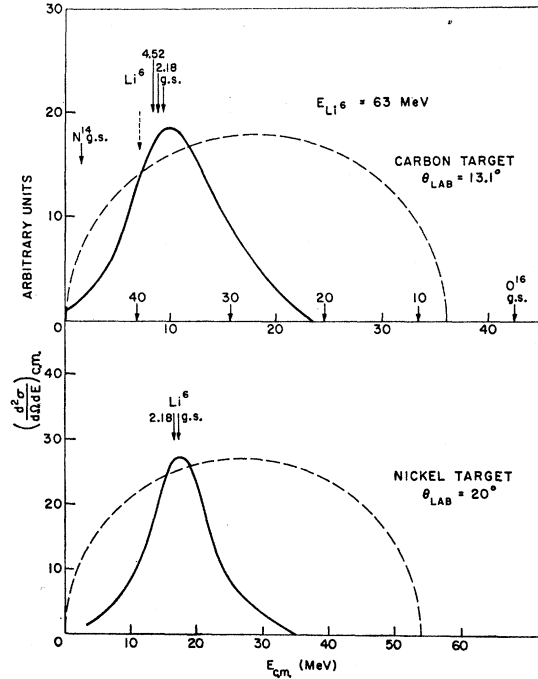


FIG. 14. Deuteron energy spectra observed in the dissociation of Li<sup>6</sup> compared to the statistical energy distribution for a three-body system.

( $\alpha + d + C^{12}$ ) system have also been indicated in Fig. 14. Deuterons resulting from the formation of states in O<sup>16</sup>, (C<sup>12</sup> +  $\alpha$ ), would appear with the energies indicated by the arrows on the energy axis; the numbers above the arrows indicate the corresponding excitation energy (MeV) in O<sup>16</sup>. The figure also indicates energies which deuterons would have if they appeared, after dissociation of the parent nucleus, with the same velocity that Li<sup>6</sup>( $\alpha + d$ ) or N<sup>14</sup>(C<sup>12</sup> +  $d$ ) nuclei would have if formed in various residual states in the interaction. In such cases, the observed deuteron energy spectrum would be broadened about the mean energy indicated, with a width dependent on the amount of energy released in dissociation as discussed above. In the lower part of Fig. 14, the corresponding deuteron energies for states in Li<sup>6</sup> scattered from nickel are indicated.

Consideration of the various two-body interactions illustrated in Fig. 14 indicate clearly that the deuterons result from dissociation of the incident Li<sup>6</sup> ion. However, this dissociation cannot be regarded as proceeding sequentially through inelastic scattering followed by decay, or indeed any other process which leaves the alpha particle and the deuteron with small relative momentum, for in that case the spatial correlation of the alpha particle and the deuteron would require the recoil carbon nucleus to appear at the conjugate center of mass angle with differential cross sections comparable to those for deuteron production: As indicated in Fig. 13, this was not the case, and it has been concluded that

<sup>20</sup> E. H. Beckner, C. M. Jones, and G. C. Phillips, Phys. Rev. **123**, 255 (1961).

the dissociation must be a more direct process as will be discussed below.

### B. Total Cross Sections

As quoted in Table I the total cross sections for  $E2$  Coulomb excitation to the 2.184-MeV,  $3^+$ , state in  $\text{Li}^6$  were calculated using the formulas and tables of Alder *et al.*<sup>21</sup> All the quantities appearing in the expression for  $E2$  Coulomb-excitation total cross sections are calculable with the exception of the reduced transition probability  $B(E2)$ . The appropriate  $B(E2)$  value for the deexcitation of the 2.184 state has not been measured and in consequence it has been necessary to estimate this indirectly. Since Coulomb effects should be most apparent for interactions with targets of high atomic number, the calculated cross sections ( $\sigma_{E2}$ ) in Table I were normalized to the experimental value given by Anderson<sup>18</sup> ( $270 \pm 40$  mb) for deuteron production from the 60.6-MeV  $\text{Li}^6$  bombardment of gold. This, in turn, provided a rough estimate of the  $B(E2)$  value, to the extent that Anderson's data are explicable as reflecting Coulomb excitation.

Comparison with the observed cross sections (Table I) indicates that the results obtained with the nickel target are not inconsistent with a Coulomb excitation mechanism. The correct energy dependence is obtained, and the absolute cross section values agree within about 10%, which is as good as might be expected considering the approximate nature of the above normalization procedure, leading to  $B(E2)$ . The cross sections for the carbon target, however, are two to three times higher than the estimated Coulomb cross sections, and do not have the expected energy dependence; in consequence it may be concluded that a specifically nuclear interaction dominates the dissociation in the lighter system.

It should also be noted for both carbon and nickel target that the differential cross sections decrease much more rapidly with angle than those predicted for Coulomb excitation. Figure II.7 in Ref. 21 indicates that the differential cross section for  $E2$  excitation falls off by at most a factor of three in the range  $0$  to  $180^\circ$ , whereas the observed cross sections decrease by at least a factor of ten in the first ninety degrees. The same qualitative discrepancy was apparent in Anderson's data, suggesting that nuclear effects must play a significant role in the heavier systems as well.

### C. Angular Distributions

The observed angular distributions, presented in Figs. 7 and 8, show none of the oscillatory structure characteristics of direct interactions; nor do they exhibit a maximum at the grazing angle  $\theta_g$ , as would be expected in a surface or grazing reaction. The results

<sup>21</sup> K. Alder, A. Bohr, T. Huus, B. Mottelson, and A. Winther, *Rev. Mod. Phys.* **28**, 432 (1956).

discussed above indicate that a direct nuclear interaction dominates the dissociation process and an attempt has been made to calculate the angular distributions to be expected with such an interaction.

In the system under consideration, an alpha particle ( $M_1$ ) and a deuteron ( $M_2$ ) are bound in the initial state and free in the final state as a result of some unspecified direct interaction with a target nucleus ( $M_3$ ). If  $\mathbf{r}$  is the relative coordinate between  $M_1$  and  $M_2$ , and if the dominant interaction is assumed to be of the form  $V(\mathbf{R})$ , where  $\mathbf{R}$  is the relative coordinate between the target nucleus ( $M_3$ ) and the center of mass of the incident ion ( $M_1+M_2$ ), then the matrix element for the transition may be written generally as

$$M = \int \Phi_f^*(\mathbf{r}) \Psi_f^*(\mathbf{R}) V(\mathbf{R}) \Psi_i(\mathbf{R}) \Phi_i(\mathbf{r}) d\mathbf{r} d\mathbf{R} \quad (9)$$

$$= \int \Phi_f^*(\mathbf{r}) \Phi_i(\mathbf{r}) d\mathbf{r} \int \Psi_f^*(\mathbf{R}) V(\mathbf{R}) \Psi_i(\mathbf{R}) d\mathbf{R}. \quad (10)$$

The second integral in Eq. (10) represents the interaction between the incident ion and the target nucleus, and may be written

$$t(\mathbf{K}) = \int \Psi_f^*(\mathbf{R}) V(\mathbf{R}) \Psi_i(\mathbf{R}) d\mathbf{R} \quad (11)$$

where  $\mathbf{K}$  is the momentum transfer involved.

The bound-state wave function has been taken as

$$\Phi_i(\mathbf{r}) = N(e^{-a\mathbf{r}}/r), \quad (12)$$

where  $N$  is a normalizing factor and

$$\alpha = (2\mu E_B)^{1/2}/\hbar; \quad (13)$$

$\mu$  is the reduced mass and  $E_B$  is the binding energy of the system ( $M_1+M_2$ ). The free final-state wave function has been approximated as a plane wave

$$\Phi_f(\mathbf{r}) = e^{i\mathbf{k}\cdot\mathbf{r}}. \quad (14)$$

Substituting Eqs. (11), (12), and (13) into Eq. (10) results in an expression for the matrix element

$$M = t(\mathbf{K}) \int e^{-i\mathbf{k}\cdot\mathbf{r}} N e^{-a\mathbf{r}} r^{-1} d\mathbf{r} \quad (15)$$

$$= t(\mathbf{K}) \frac{4\pi N}{\alpha^2 + k^2}. \quad (16)$$

In order to obtain numerical results, the form of the nuclear interaction  $t(\mathbf{K})$  must be known. As a simple approximation, which should serve to indicate the gross properties of this analysis, a simple elastic diffraction scattering model has been utilized. The form which was found most successful in fitting data for the elastic scattering of 40-MeV alpha particles from carbon is

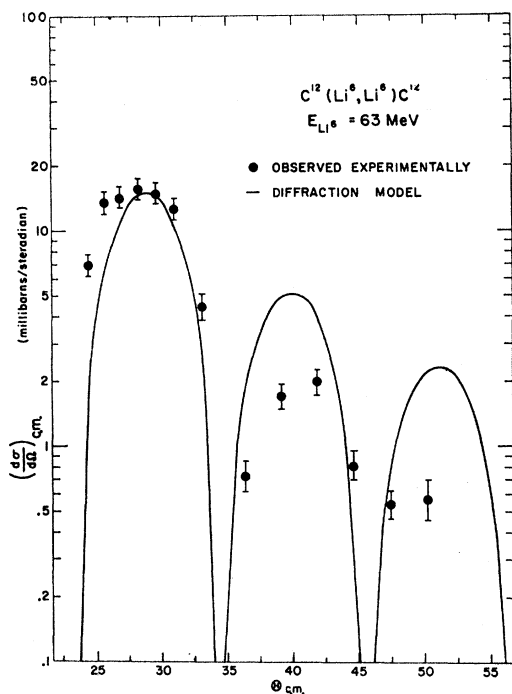


FIG. 15. Angular distribution observed in the elastic scattering of  $\text{Li}^6$  by  $\text{C}^{12}$  compared to the diffraction model discussed in the text.

given by Yavin and Farwell<sup>22</sup> as

$$|t(\mathbf{K})|^2 \sim K^2 R^4 \cos^2(\theta/2) \left[ \frac{J_1[2KR \sin(\theta/2)]}{2KR \sin(\theta/2)} \right]^2. \quad (17)$$

As indicated in Fig. 15, this form for the differential cross section, normalized to the *first* observed maximum, provides qualitative agreement with at least the positions of the diffraction maxima observed here in the elastic scattering of  $\text{Li}^6$  by carbon, with the value of  $R$  required to fit the data given by  $R = 1.48(A_1^{1/3} + A_2^{1/3})F$ . It should be pointed out that since the forward center-of-mass angles (smaller than  $\theta_{lab} = 8.5^\circ$ ) were experimentally inaccessible in the scattering of  $\text{C}^{12}$  by lithium due to the large center-of-mass motion and the scattering chamber limitations, the observed angular distribution in fact excludes the first two maxima of the diffraction oscillations and the above normalization has been made accordingly.

Using this form for  $|t(\mathbf{K})|^2$ , and assuming that  $M$  depends only on the directions of the momenta involved,

$$\frac{d^2\sigma}{d\Omega_\phi d\Omega_\theta} \sim |M|^2 \sim \left[ \frac{\cot(\theta/2) J_1[2KR \sin(\theta/2)]}{\alpha^2 + k^2} \right]^2 = \left[ \frac{\cot(\theta/2) J_1[2KR \sin(\theta/2)]}{\alpha^2 + K^2 + 4k_d^2 - 4k_d K \cos(\theta - \phi)} \right]^2, \quad (18)$$

<sup>22</sup> A. I. Yavin and G. W. Farwell, Nucl. Phys. **12**, 1 (1959).

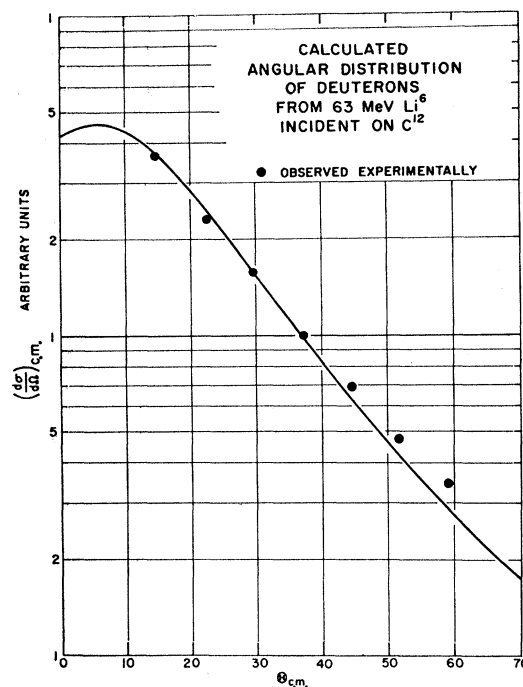


FIG. 16. Calculated angular distribution of deuterons from the dissociation of 63-MeV  $\text{Li}^6$  ions incident on a carbon target, compared to the experimental data.

where  $\theta$  is the scattering angle of the effective  $\text{Li}^6$  ion (center of mass of  $m_1$  and  $m_2$ ), and  $\phi$  is the scattering angle of the deuteron ( $m_2$ );  $\mathbf{K} = \mathbf{k}_\alpha + \mathbf{k}_d$  and  $\mathbf{k} = \mathbf{k}_\alpha - \mathbf{k}_d$ . The predicted deuteron angular distribution was obtained by integrating Eq. 18 over all scattering directions  $d\Omega_\phi$ . The integral was calculated numerically for the desired range of  $\phi$  using an IBM 709 computer. The "elastic" values of  $K$  and  $k_d$ , (i.e.,  $k_d = \frac{1}{3}K$ ) were used, and the same value of  $R$  used to fit the elastic scattering data was also used in these calculations.

The results are presented in Figs. 16–19, with the calculated distributions normalized to the experimental data at one point in each case. It is gratifying that this simple analysis does reproduce the general features observed experimentally. Any diffraction oscillations present in the original or intrinsic scattering interactions are averaged out by integration over the scattering angle, so that the differential cross section of the dissociation product varies smoothly with angle. The relative insensitivity of the shape of the distribution to the incident energy is also reproduced. The change in slope between the angular distributions for the carbon and nickel targets is obtained. The least satisfactory fit is that found in the low energy case for nickel, where it has been noted above that Coulomb effects, neglected in this analysis, may be expected to enter most strongly. The best fit is found for the highest incident  $\text{Li}^6$  energy on carbon, where nuclear effects are expected to be most important.

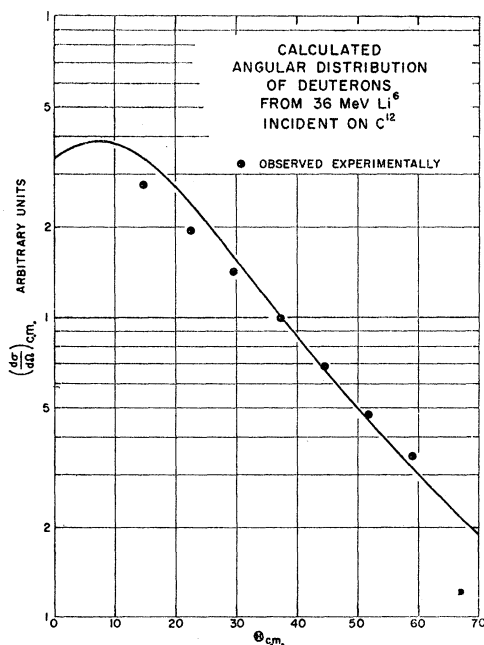


FIG. 17. Calculated angular distribution of deuterons from the dissociation of 36-MeV  $\text{Li}^6$  ions incident on a carbon target, compared to the experimental data.

The diffraction breakup of light nuclei by purely nuclear interactions has been calculated by Sitenko and Berezhnoi<sup>23</sup> to be approximately independent of incident energy. This has been observed here in the interaction of  $\text{Li}^6$  ions with the carbon target. The energy dependence of the cross sections is most probably due to Coulomb effects in the case of nickel target.

In order to examine further, the relative importance of the nuclear and Coulomb interactions, the simple nuclear model characterized by Eq. (18) has also been applied to the earlier measurements for 60.6- and 33.5-MeV  $\text{Li}^6$  ions on gold.<sup>18</sup> No agreement was obtained; whereas the experimental angular distributions peaked at angles of approximately 25 and 80°, respectively, in the laboratory, the calculated angles were approximately 3 and 4°, respectively. This disagreement further supports the contention that the dissociation observed in  $\text{Li}^6$  interactions with heavy targets is dominated by sequential Coulomb excitation and decay as suggested by Gluckstern and Breit.<sup>19</sup> In the case of a nickel target, both nuclear and Coulomb forces play a role and in that of a carbon target the nuclear effects are dominant.

Inspection of Eq. (18) shows that for a given lithium scattering angle  $\theta$ , the product deuteron can appear at any angle  $\phi$ , with cross section which is a maximum for  $\phi = \theta$  but which is still significant for all values of  $\phi$ . Since the major contribution to diffraction scattering is contained in the first maximum, a large fraction of the

carbon nuclei which contribute to this direct dissociation would appear at small recoil angles, while the product deuterons would be spread over a wide range of angles. This would account for the observed discrepancy between the cross sections for deuteron production and inelastically scattered carbon ions (Fig. 13), since the extreme forward center-of-mass angles were not observed.

Since it is possible that interactions between the target nucleus and the individual cluster components might also be of importance, similar calculations have been performed assuming that the alpha particle and the deuteron scatter incoherently as free particles. The angular distribution of the deuterons resulting from the "free" scattering of alpha particles was calculated using the same direct diffraction model discussed above. The free scattering of deuterons from  $\text{C}^{12}$  has been observed<sup>24</sup> to oscillate about the Rutherford scattering cross section in a manner typical of such interactions. Since the complex interaction considered here would not be expected to exhibit sharp diffraction effects (the deuteron energy is not unique, for one thing), the "free" deuteron scattering was represented by the Rutherford angular dependence in making the calculations. This, in effect, averaged over the diffraction oscillations.

The results of this calculation are presented in Fig. 20. The three curves shown were normalized individually

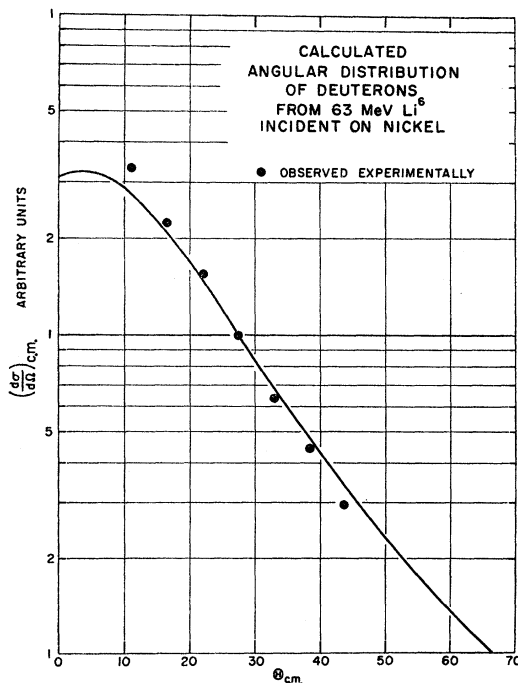


FIG. 18. Calculated angular distribution of deuterons from the dissociation of 63-MeV  $\text{Li}^6$  ions incident on a nickel target, compared to the experimental data.

<sup>23</sup> A. G. Sitenko and Iu. A. Berezhnoi, Zh. Eksperim. i Teor. Fiz. 35, 1289 (1958) [English transl.: Soviet Phys.—JETP 8, 899 (1959)].

<sup>24</sup> R. G. Freemantle, W. M. Gibson, and J. Rotblat, Phil. Mag. 45, 1200 (1954); R. J. Slobodrian, Phys. Rev. 125, 1003 (1962).

to the experimental data at one point. The fit to the observed angular distribution is seen to be quite good at large angles, but rises much too steeply at forward angles. The assumed scattering of the  $\text{Li}^6$  center of mass as a unit (Figs. 16–19) gave a significantly better fit to the data over the entire angular range, and thus represents the best description thus far available for the observed direct dissociation mechanism.

### V. SUMMARY AND CONCLUSIONS

Contrary to expectations, no evidence has been found for deuteron groups corresponding to formation of states in  $\text{O}^{16}$  resulting from interactions between high-energy  $\text{Li}^6$  ions and a carbon target. It has been found that binary dissociation into an alpha particle and deuteron dominates  $\text{Li}^6$  interactions at these energies, indicating that it may be very difficult, if not impossible, to obtain information of a spectroscopic nature utilizing high-energy lithium beams. The results indicate that a specifically nuclear interaction which leaves the dissociation products uncorrelated must dominate the dissociation mechanism, at least for light nuclei. Angular distributions calculated on the assumption that the dissociation was induced by direct nuclear scattering of the  $\text{Li}^6$  complex by the target were in qualitative agreement with the experimental data. The large cross sections observed for such a direct dissociation of  $\text{Li}^6$  into an alpha particle and a deuteron lend support to

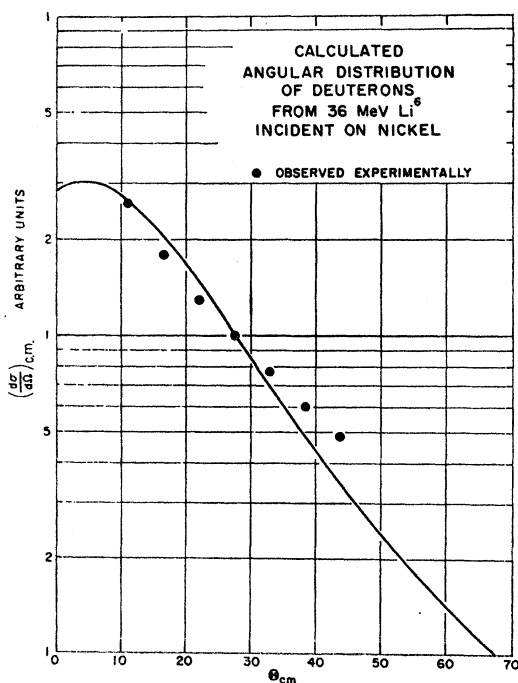


FIG. 19. Calculated angular distributions of deuterons from the dissociation of 36-MeV  $\text{Li}^6$  ions incident on a nickel target, compared to the experimental data.

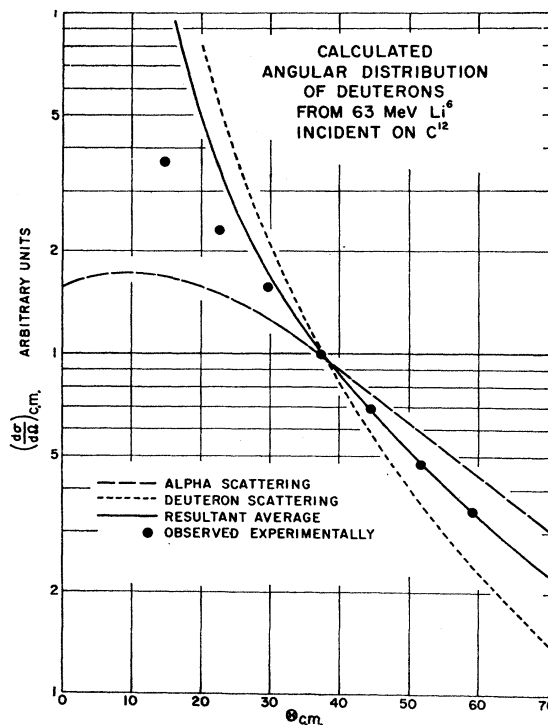
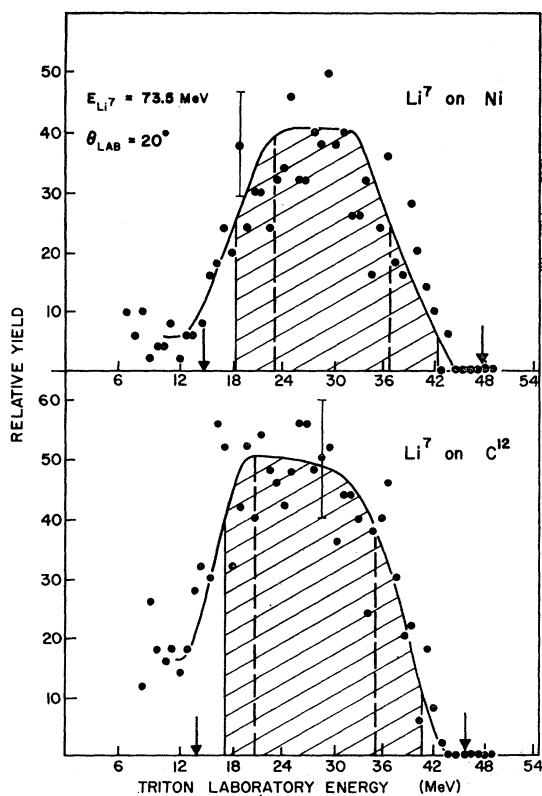


FIG. 20. Calculated partial and total differential cross sections of deuterons from the dissociation of 63-MeV  $\text{Li}^6$  ions incident on a carbon target.

the corresponding cluster model description of this nucleus.

### APPENDIX I

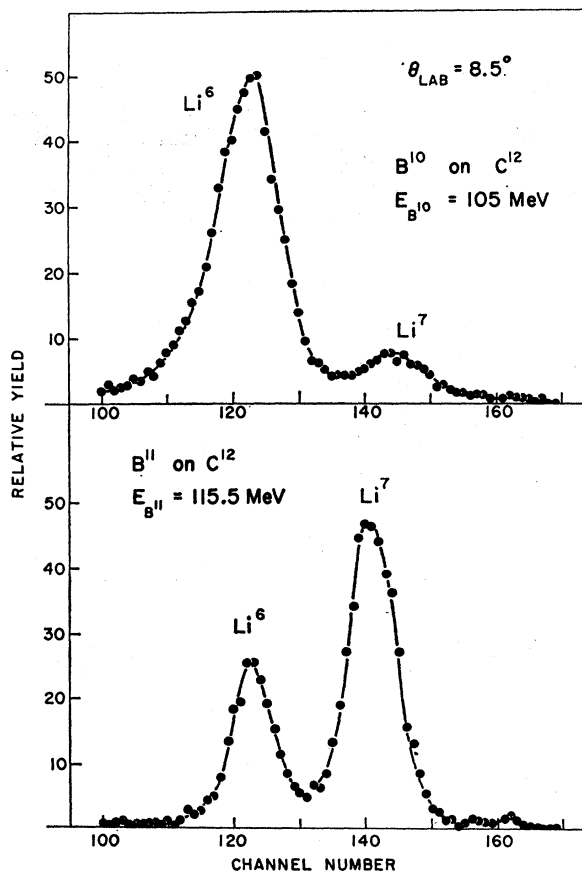
Because of instrumental difficulties in the acceleration of a  $\text{Li}^7$  beam during the course of the work reported herein, only preliminary data were obtained on the dissociation of  $\text{Li}^7$ . Triton energy spectra from the dissociation of  $\text{Li}^7$  are shown in Fig. 21, and have the same general shape observed in the deuteron spectra from  $\text{Li}^6$ . The shaded areas have the same significance here as those in the deuteron energy spectra of Figs. 5 and 6, assuming that dissociation proceeds via the 4.63-MeV state in  $\text{Li}^7$ . This is the first-particle unstable state in  $\text{Li}^7$ , lying 2.16 MeV above the threshold for dissociation into an alpha particle and triton. The arrows in Fig. 21 indicate the predicted width for dissociation following excitation of  $\text{Li}^7$  to its next higher level, at 6.54 MeV, 4.07 MeV above the dissociation threshold; the dashed lines indicate the width shown previously in the deuteron energy spectra, corresponding to an energy release of 0.71 MeV. The spectrum width is quite sensitive to excitation, and the fact that the triton spectra are wider than the deuteron spectra suggests that the dissociation proceeds only when the effective excitation is in the neighborhood of an unbound state, even though as shown herein, the three-body nuclear interaction leading to dissociation need not proceed sequentially through isolated excited states.

FIG. 21. Triton energy spectra from the dissociation of  $\text{Li}^7$ .

The triton yield at this angle of observation was roughly one-half of the corresponding deuteron yield from the dissociation of  $\text{Li}^6$ . In the  $\text{Li}^6$  interactions, the yield of tritons was negligible compared to the deuteron yield, whereas in the  $\text{Li}^7$  interactions the deuteron and triton yields were roughly equal. This result is in accord with the recent measurements of Ruhla *et al.*<sup>11</sup> on the  $(p, pd)$  and  $(p, pt)$  reactions. Since the emission of tritons from  $\text{Li}^6$  would require dissociation of the alpha-particle core, whereas both tritons and deuterons may be removed from  $\text{Li}^7$  leaving this core intact, it would be premature to reach any conclusion on the basis of these data regarding the cluster structure of  $\text{Li}^7$ .

#### APPENDIX II

The binary dissociation of  $\text{B}^{10}$  and  $\text{B}^{11}$  ions interacting with carbon and nickel targets into alpha particles and lithium isotopes was also observed. Figure 22 presents sections of multiplier spectra corresponding to these observations, illustrating the isotopic separation attained. A small yield of  $\text{Li}^8$  ions from these reactions is evident in the figure. The relative yield of  $\text{Li}^6$  and  $\text{Li}^7$  illustrated here is typical of all measurements made with boron beams and demonstrates, as in the lithium case, that the conjugate alpha particle, by virtue of its

FIG. 22. Multiplier pulse-height spectra of the lithium isotopes observed in boron reactions with  $\text{C}^{12}$ .

high internal binding, is a preferred cluster in the dissociation of light nuclei.

The  $\text{Li}^6$  and  $\text{Li}^7$  energy spectra show the characteristic dissociation shapes, as indicated in Fig. 23. In the lower part of this figure the vertical bar marks the energy which a  $\text{Li}^7$  ion would have if it had the same velocity as a  $\text{B}^{11}$  ion inelastically scattered with  $Q = -8.67$  MeV, the energy required for dissociation. There are many levels in  $\text{B}^{11}$  available in the energy region above this excitation, and the  $\text{Li}^7$  spectrum does indicate a maximum yield at this "constant velocity" energy.

No equivalently simple explanation appears valid for the  $\text{B}^{10}$  dissociation data, also shown here, since the "constant velocity" energies for dissociation of either  $\text{B}^{10}$  or  $\text{C}^{12}$ , as indicated on the figure, do not correspond to the observed maximum in the  $\text{Li}^6$  energy spectrum. It would be anticipated *a priori* that the contribution from carbon dissociation ( $\text{C}^{12} \rightarrow 2\text{Li}^6$ ) would be relatively small, since the dissociation energy is 28.2 MeV as compared to 4.46 MeV in  $\text{B}^{10}$ .

Total dissociation cross sections were obtained from preliminary angular distributions, shown here in Fig. 24. The results obtained were 49 mb (3.8% of the geometric

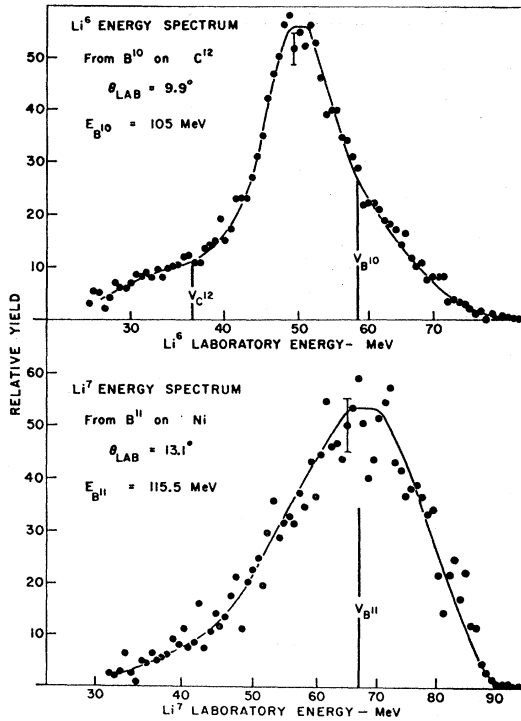


FIG. 23. Energy spectra of lithium isotopes observed in the dissociation of boron ions.

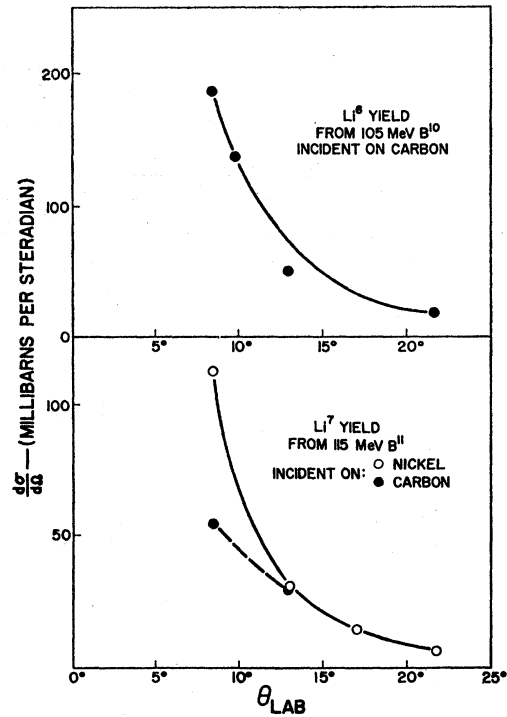


FIG. 24. Angular distributions of lithium isotopes observed in the dissociation of boron ions.

cross section) for the production of  $\text{Li}^6$  in the  $\text{B}^{10} + \text{C}$  interaction and 32 mb (1.3% of geometric) for  $\text{Li}^7$  from the  $\text{B}^{11} + \text{Ni}$  interaction. The small fractional branching into the dissociation channel reflects the higher energies, hence a larger number of open-exit channels involved.

In view of the high probability for dissociation of  $\text{Li}^6$  in nuclear encounters, noted above, it is surprising that the yield of  $\text{Li}^6$  from the  $\text{B}^{10}$  reactions should be even as large as it is, supporting the hypothesis that

the  $\text{B}^{10}$  wave function has a significant  $(\text{Li}^6 + \alpha)$  binary cluster amplitude.

#### ACKNOWLEDGMENTS

The authors are indebted to M. Sachs, J. Poth, and K. Nagatani for their assistance in the experimental measurements. They would also thank Professor T. A. Tombrello and Professor K. R. Greider for many stimulating discussions concerning the interpretation of the data presented.

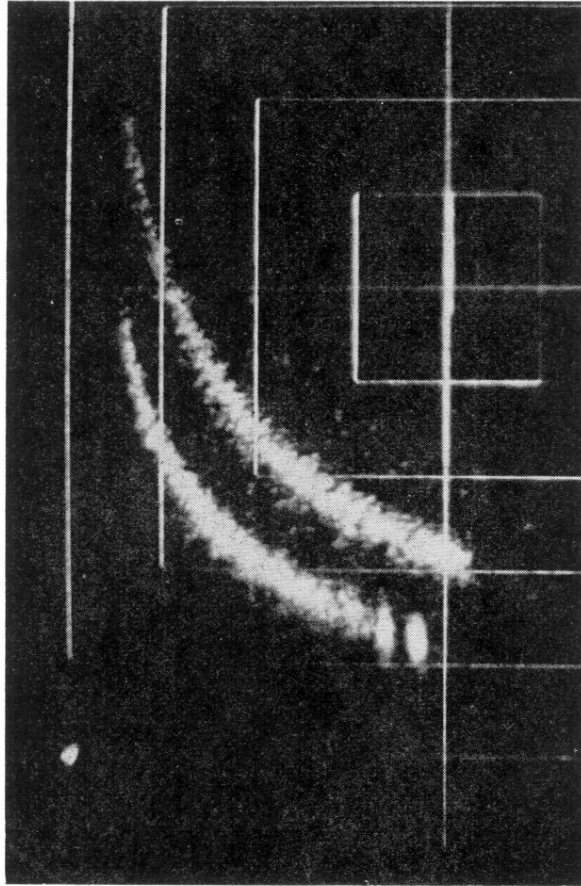


FIG. 2. Plotting oscilloscope photograph of  $\Delta E$  versus  $E$  for the 63-MeV  $\text{Li}^6$  bombardment of a polythene ( $\text{CH}_2$ ) target. Much longer exposure times would have been required to show a similar triton locus. (See Fig. 3.)

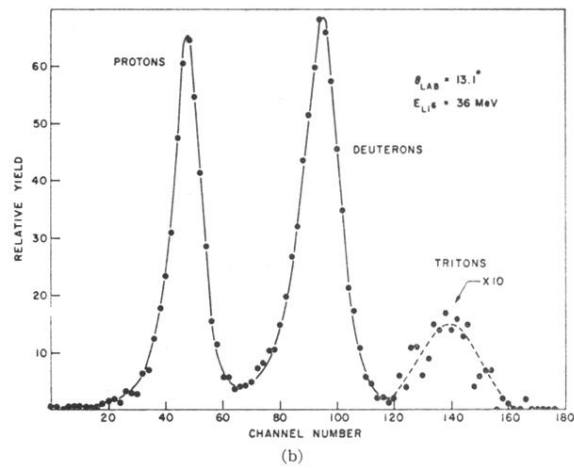
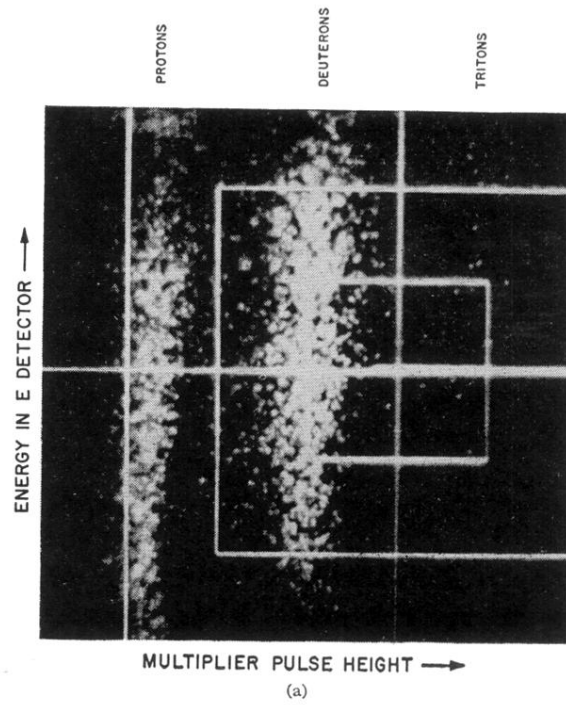


FIG. 3. (a) Oscillographic and (b) spectra displays of the multiplier response to the hydrogen isotopes produced in the 36-MeV  $Li^6$  bombardment of  $C^{12}$ .